Thomson Reuters Master Journal List JOURNAL LIST

Search terms: INTERNATIONAL TRANSACTIONS ON ELECTRICAL ENERGY SYSTEMS
Total journals found: 1

1. INTERNATIONAL TRANSACTIONS ON ELECTRICAL ENERGY SYSTEMS
Bimonthly ISSN: 2050-7038
WILEY-BLACKWELL, 111 RIVER ST, HOBOKEN, USA, NJ, 07030-5774

1. Science Citation Index Expanded
2. Current Contents - Engineering, Computing & Technology

INTERNATIONAL TRANSACTIONS ON ELECTRICAL ENERGY SYSTEMS
Int. Trans. Electr. Energ. Syst. (2014)
Published online in Wiley Online Library (wileyonlinelibrary.com). DOI: 10.1002/etep.1906

Optimum generation dispatching of distributed resources in smart grids

Meghdad Ansarian[1]*,†, Seyed Mohammad Sadeghzadeh[2] and Mahmud Fotuhi-Firuzabad[3]

[1] *Department of Electrical Engineering, Science and Research Branch, Islamic Azad University, Tehran, Iran*
[2] *Department of Electrical Engineering, Shahed University, Tehran, Iran*
[3] *Department of Electrical Engineering, Sharif University of Technology, Tehran, Iran*

SUMMARY

Increasing interest in smart grids exhibits its potential benefits for providing reliable, secure, efficient, environmental friendly and sustainable electricity from renewable energy resources. Here, reliability models of four types of renewable and hybrid distributed generation were developed. A fuzzy multi-objective function was suggested for simultaneous optimization of reliability, electricity generation cost, grid loss and voltage profile. This not only considers uncertainty of renewable energy resources but also provides smart generation dispatching. An efficient reliability index consisting of energy and interruption frequency terms was also defined. A novel hybrid heuristic optimization method based on simulated annealing and particle swarm optimization methods was proposed. These approaches were applied to the generation dispatching of a smart grid, and the results were discussed in details. Scenarios including the changes of wind speed, sun light, fuel price and weight coefficients of the objective function were analyzed. This work succeeds to model uncertainty of renewable energy resources and performs technical and economical optimization in the power generation planning. Copyright © 2014 John Wiley & Sons, Ltd.

KEY WORDS: renewable energy resources; smart grids; generation dispatching; reliability; multi-objective function; heuristic optimization techniques

1. INTRODUCTION

The high service reliability, high power quality, low cost, energy efficiency enhancement, energy independence and employing renewable energies are the most interesting factors in the utilization of distributed energy resources (*DER*). An approach for implementing *DER*s along with high-tech control and communication devices is called smart grid, which causes significant improvement in the power system operating conditions [1]. Smart micro grid is a concept which refers to a small-scale power system including a cluster of loads and distributed generations (*DG*) operating together based on energy management, control and protection devices accompanied by the related software to support future power grids. Smart micro grids can operate in connection to the power system or as an isolated one. In both conditions, the whole generation units and load points are manipulated by a monitor and control center [2–5]. For considering uncertainty of wind energy, Dobakhshari and Fotuhi-firuzabad [6] suggested a reliability model of a wind turbine (*WT*) farm. In this paper, a similar model to the suggested one is used for a single *WT*. Moreover, we have developed reliability models for three types of renewable and hybrid *DGs*. The approach has overcome the setbacks associated with simulation-based methods in terms of both volume of data and computational burden of such techniques.

By integrating *DER*s, common formulation of generation dispatching problem should be modified [7]. An energy management system based on mixed integer nonlinear programming and a local energy market

*Correspondence to: Meghdad Ansarian, Department of Electrical Engineering, Science and Research Branch, Islamic Azad University, Tehran, Iran.
†E-mail: ansarian@iausr.ac.ir

are presented for a micro grid [8]. Furthermore, an architecture for real-time operation for an islanded micro grid is suggested to find out hourly power set points of *DER*s and customers [9]. It is obvious that there is an essential need for sharp dispatching of power generations in a smart grid that is helpful to improve the grid operation. This necessitates the development of more reliable power dispatching and optimization methods. Classical optimization techniques such as linear and quadratic programmings exploit several approximations in order to reduce optimization complexity problem. In addition, those techniques are highly sensitive to the starting points with large probability of convergence at local optima. Those are usually used for specific optimization cases and do not offer great degree of freedoms in the objective functions or types of constraints [10]. The importance of applying heuristic optimization techniques for short-term energy planning is mainly due to the existence of multiple uncertainties [11]. The *PSO* method has been significantly employed in the optimal operation management regarding its population-based search capability, convergence speed and robustness. However, the performance of a conventional *PSO* algorithm gives rise to local optima trapping [12,13]. Therefore, a novel hybrid heuristic optimization method was developed based on *SA* and *PSO* techniques, in this study. The combination called *SA–PSO* method gains the global optimization from *SA* and the advantages regarding the *PSO*.

In order to achieve an optimal generation dispatching, four technical and economic objectives consisting of power supply reliability, *EGC*, *GL* and *VP* were simultaneously optimized via an *FMOF*. Furthermore, a reliability index including the energy and interruption frequency terms was defined and subsequently applied to the generation dispatching. A case study was investigated, and the results were discussed in detail.

2. DURATION AND FREQUENCY CONCEPTS IN TIME SERIES

Available quantity of renewable energies such as wind and solar irradiance determine power generated by renewable *DG* units. Since these energies have random nature, actual power generation capacity of a renewable *DG* unit can be modeled as a stochastic parameter.

Markov's model could be used to describe a stochastic process as the transitions between probable states, in which each represents a discrete value. Modeling a stochastic process by a Markov model requires the residual time of state to follow an exponential distribution [6,14,15]. Here, the exponential time of state was considered for all applications. In the exponential distribution, a constant transition rate between states i and j, λ_{ij}, is given by:

$$\lambda_{ij} = \frac{N_{ij}}{T_i} \tag{1}$$

where N_{ij} is the number of observed transitions from state i to state j, and T_i denotes the duration of state i calculated during the whole period.

The departure rate from state i to the upper and lower states ascertained to be λ_{+i} and λ_{-i}, respectively, is as follows:

$$\lambda_{+i} = \sum_{j=1, j>i}^{N_{states}} \lambda_{ij} \tag{2}$$

$$\lambda_{-i} = \sum_{j=1, j<i}^{N_{states}} \lambda_{ij} \tag{3}$$

where N_{states} is the total number of states.

Occurrence probability of state i, P_i, is as Equation (4):

$$P_i = \frac{T_i}{\sum_{j=1}^{N_{states}} T_j} = \frac{T_i}{T} \tag{4}$$

where T is the entire period of observation.

DOI: 10.1002/etep

The frequency of occurrence of state i, f_i, is as below:

$$f_i = P_i(\lambda_{+i} + \lambda_{-i}) \tag{5}$$

3. RELIABILITY MODELS OF RENEWABLE DG UNITS

Nowadays, renewable energy resources face public attraction due to being distributed in most places, environmental friendly and fuel cost vanishing. Since these power sources are related to uncertain energy resources, it is customary to exploit the auxiliary energy source to develop a hybrid generation unit. A few possible options are available that can adapt themselves in conjunction with a *WT* or photovoltaic (*PV*) array. Those are fuel cell (*FC*), batteries, reciprocating generators and micro turbines. Batteries are desirable for a short-term solution. Reciprocating generators and micro turbines offer a compact size and high energy density; however, those are pollutants and their running cost is high. Despite the solar and wind energies are renewable; however, their combination looks like not to be reliable. *FCs* possess high clean energy densities, which generate power as long as the fuel is supplied. Although *FC*s have higher fuel costs, because of their higher efficiencies, their performance resembles to be much better than the reciprocating engines [16]. In general, renewable *DG*s given in the present work include *WT*, *PV*, hybrid *WT–FC* and hybrid *PV–FC*. Reliability model of a WT farm is developed previously [6]. A similar model is applied for a single *WT* in this paper. Moreover, we proposed three reliability models for *PV*, *WT–FC* and *PV–FC*.

3.1. WT reliability model

The output power of a *WT* depends on its turbine availability and wind speed. This model is different from non-renewable power generation units. For a non-renewable unit, it is assumed that the unit delivers its rated power when it is available. In the case of a *WT*, if it is in an operative state, its output power depends on wind speed. *WT* manufactures usually present the relationship between wind speed and output power as a power curve of the turbine. Also, output power of a *WT* is given as a function of wind speed [17] such that:

$$P = \begin{cases} 0 & v < v_{in}, v > v_{out} \\ \frac{1}{2} c_v \rho A v^3 + k & v_{in} \leq v \leq v_r \\ P_r & v_r \leq v \leq v_{out} \end{cases} \tag{6}$$

where v is wind speed, v_{in}, v_r and v_{out} represent cut-in speed, rated speed and cut-out speed of the *WT*, respectively; c_v, ρ and A ascertain total efficiency of wind power, air density and sweep area of the *WT* rotor, respectively.

A 600-kW *WT* is investigated. Figure 1 depicts the power curve of the turbine with cut-in speed, rated speed and cut-out speed of 4, 15 and 25 m/s, respectively.

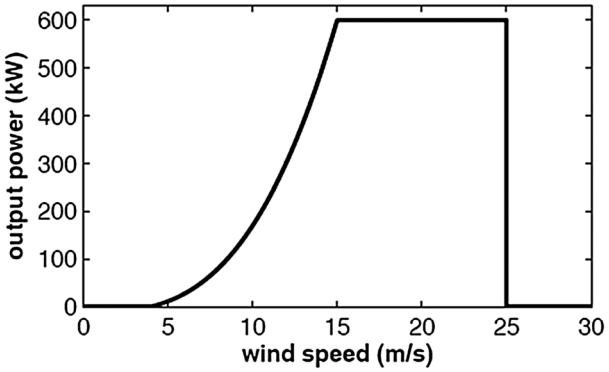

Figure 1. Reliability model of the hybrid WT–FC unit.

DOI: 10.1002/etep

When the wind speed lies between rated and cut-out speeds, rated power would be generated. Conversely, when the wind speed is either lower than the cut-in speed or higher than the cut-out speed, then the output power of the turbine would be zero. To develop the reliability model of the *WT*, the output power is split into finite states. However, the number of states is arbitrary and depends on the required accuracy of the model. For example, the output power of the 600-kW turbine can be split into five state, i.e. 0, 150, 300, 450 and 600 kW.

A wind speed sequence of 140 h is shown in Figure 2, and corresponding data for the output power result are shown in Figure 3.

The measured power in Figure 3 is depicted by dash line whereas the approximate curve exhibits the output power categorized in five finite steps.

To accommodate rapid variations in hourly wind speed, it is useful to study the possible transitions between power states. A five-state reliability model of the *WT* is proposed as shown in Figure 4, such that the steps WT_1 to WT_5 represent 600, 450, 300, 150 and 0 kW for the *WT*, respectively.

This *WT* possesses a forced outage rate (*FOR*) of 3.3%. Using Equation (1) and the *FOR*, transition matrix of the *WT*, λ_{WT}, can be obtained as follows:

$$\lambda_{WT} = \begin{bmatrix} 0 & 0.0417 & 0.0069 & 0.0069 & 0.0072 \\ 0.0347 & 0 & 0.0278 & 0 & 0.0002 \\ 0.0280 & 0.0208 & 0 & 0 & 0.0140 \\ 0.0139 & 0 & 0.0208 & 0 & 0.0140 \\ 0.0069 & 0.0048 & 0.0034 & 0.0394 & 0 \end{bmatrix} \tag{7}$$

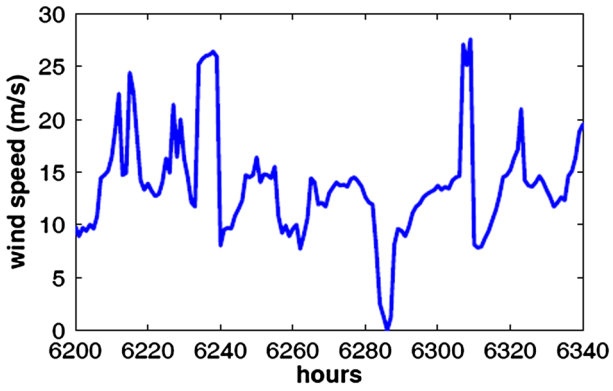

Figure 2. Reliability model of the hybrid PV–FC unit.

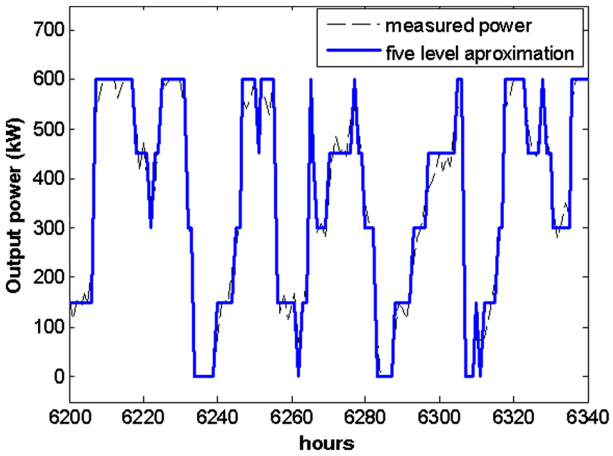

Figure 3. Smart grid case study.

DOI: 10.1002/etep

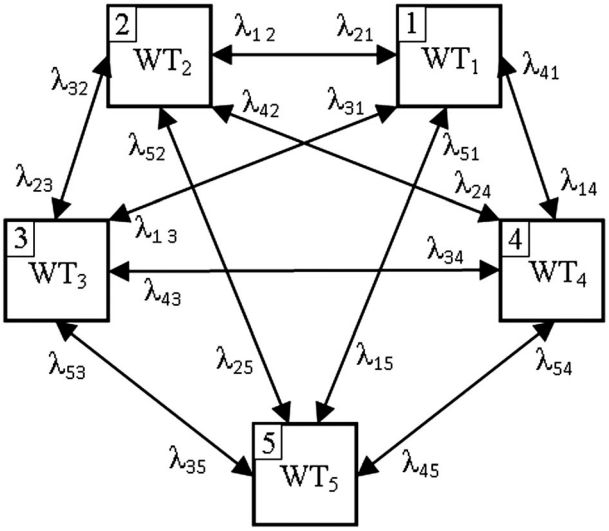

Figure 4. Power curve of the 600-kW *WT*.

3.2. *PV reliability model*

The *PV* benefits direct conversion of sunlight into electricity without interference of any heat engine. *PV* devices are robust, simply designed and require little maintenance. The prominent *PV* advantage is its construction as standalone systems to give outputs ranging microwatts to megawatts. Modeling and corresponding relations of the *PV* sources have been previously described [18–22]. Using the acquired knowledge of former articles, a reliability model for *PV* sources was developed in this work. Durisch et al. [18] reported a method for calculating energy yield of the modules according to a semi-empirical efficiency function, taking into account three parameters, namely cell temperature, solar irradiance and relative air mass. The given yield power of *mSi BP585F PV* module was adopted to use in the present calculations for a couple of days in different ambient conditions clear and cloudy weathers [18]. Furthermore, the *PV* array output power can be split into finite states, for instance 0, 110, 220 and 330 kW in the case of 330-kW *PV* array.

The output power logging of the 330-kW *mSi BP585F PV* module for 2 days (clear and cloudy skies) operation is shown in Figure 5. The measured curve corresponds to the exact generation of output power, and the approximate one shows the output power piece wisely divided in the finite steps.

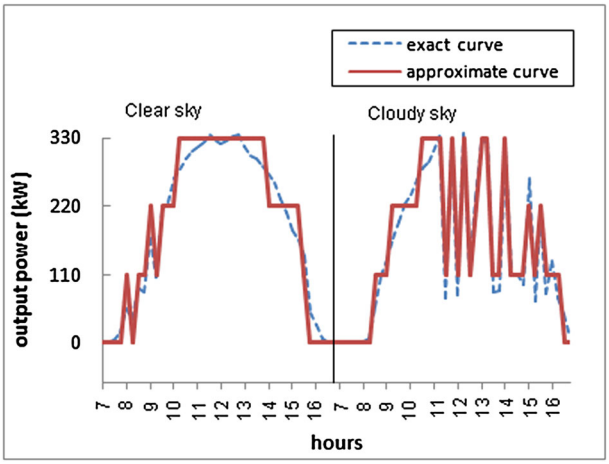

Figure 5. Instantaneous wind speed during 140 h.

DOI: 10.1002/etep

A four-state reliability model of the *PV* array was developed as shown in Figure 6, such that PV_1 to PV_4 represent 300, 220, 110 and 0 kW output, respectively.

Equation (1) is written based on this *PV* unit with *FOR* of 0.45% to obtain the corresponding transition matrix, λ_{PV} as below:

$$\lambda_{PV} = \begin{bmatrix} 0 & 0.025 & 0.125 & 0 \\ 0.075 & 0 & 0.100 & 0 \\ 0.075 & 0.150 & 0 & 0.075 \\ 0 & 0 & 0.075 & 0 \end{bmatrix} \tag{8}$$

3.3. Hybrid WT–FC

A proton exchange membrane (*PEM*) type of *FC* was considered in this study because of its faster transient response comparing other types of *FC*s as well as grid connection ability [23]. Hence, when

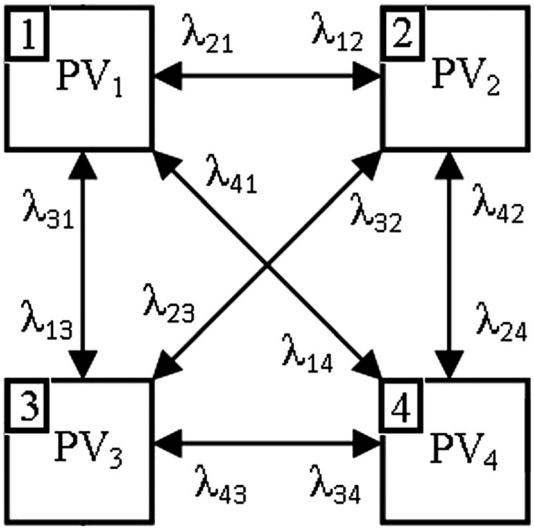

Figure 6. Instantaneous output based on measurements and approximations.

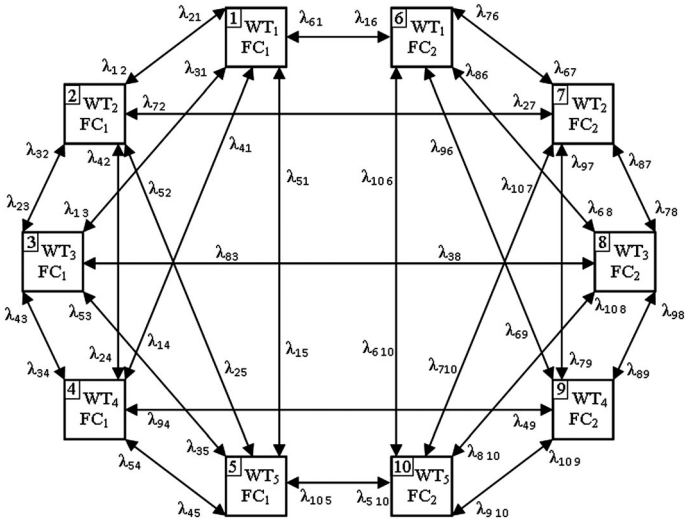

Figure 7. Reliability model of the *WT*.

DOI: 10.1002/etep

the *FC* is available, it is utilized in full capacity. The corresponding reliability model consists of two states: FC_1 when it is available, and FC_2 during failure. *WT* of the hybrid unit is the same as that discussed in section 3.1. Therefore, the reliability model of the hybrid *WT–FC* unit arises from the combination of reliability models of the *WT* and the *FC*, where the hybrid *WT–FC* unit involves ten states according to Figure 7.

The transition matrix of a *PEM* type of *FC*, λ_{FC}, in terms of occurrence/hour is given in Equation (9):

$$\lambda_{FC} = \begin{bmatrix} 0 & 0.0003 \\ 0.0333 & 0 \end{bmatrix} \tag{9}$$

Regarding λ_{WT} in Equation (7) and λ_{FC} in Equation (9), the transition matrix of the *WT–FC*, λ_{WT-FC} is obtained according to the following form:

$$\lambda_{WT-FC} = \begin{bmatrix} 0.0000 & 0.0417 & 0.0069 & 0.0069 & 0.0072 & 0.0003 & 0.0000 & 0.0000 & 0.0000 & 0.0000 \\ 0.0347 & 0.0000 & 0.0278 & 0.0000 & 0.0002 & 0.0000 & 0.0003 & 0.0000 & 0.0000 & 0 .0000 \\ 0.0208 & 0.0208 & 0.0000 & 0.0000 & 0.0140 & 0.0000 & 0.0000 & 0.0003 & 0.0000 & 0.0000 \\ 0.0139 & 0.0000 & 0.0208 & 0.0000 & 0.0140 & 0.0000 & 0.0000 & 0.0000 & 0.0003 & 0.0000 \\ 0.0069 & 0.0048 & 0.0034 & 0.0394 & 0.0000 & 0.0000 & 0.0000 & 0.0000 & 0.0000 & 0.0003 \\ 0.0333 & 0.0000 & 0.0000 & 0.0000 & 0.0000 & 0.0000 & 0.0417 & 0.0069 & 0.0069 & 0.0072 \\ 0.0000 & 0.0333 & 0.0000 & 0.0000 & 0.0000 & 0.0347 & 0.0000 & 0.0278 & 0.0000 & 0.0002 \\ 0.0000 & 0.0000 & 0.0333 & 0.0000 & 0.0000 & 0.0208 & 0.0208 & 0.0000 & 0.0000 & 0.0140 \\ 0.0000 & 0.0000 & 0.0000 & 0.0333 & 0.0000 & 0.0139 & 0.0000 & 0.0208 & 0.0000 & 0.0140 \\ 0.0000 & 0.0000 & 0.0000 & 0.0000 & 0.0333 & 0.0069 & 0.0048 & 0.0034 & 0.0394 & 0.0000 \end{bmatrix} \tag{10}$$

3.4. Hybrid PV–FC reliability model

A hybrid *PV–FC* source consists of a *PV* and an *FC* as discussed in previous sections is applied. Figure 8 depicts the reliability model of the hybrid *PV–FC* unit.

Considering λ_{PV} in Equation (8) and λ_{FC} in Equation (9), the transition matrix of the hybrid *PV–FC* unit, λ_{PV-FC}, is represented by:

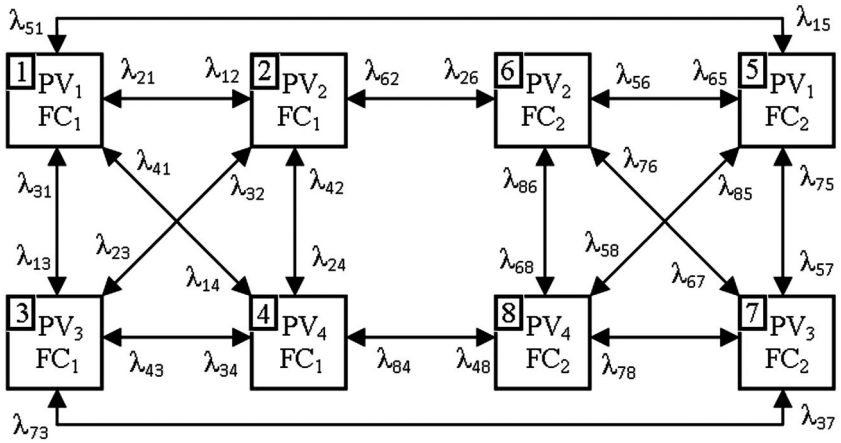

Figure 8. Output power logging for a 330-kW *mSi BP585F PV* array during 2 days operating (clear and cloudy sky).

DOI: 10.1002/etep

$$\lambda_{PV-FC} = \begin{bmatrix} 0.0000 & 0.0250 & 0.01250 & 0.0000 & 0.0003 & 0.0000 & 0.0000 & 0.0000 \\ 0.0750 & 0.0000 & 0.1000 & 0.0000 & 0.0000 & 0.0003 & 0.0000 & 0.0000 \\ 0.0750 & 0.1500 & 0.0000 & 0.0750 & 0.0000 & 0.0000 & 0.0003 & 0.0000 \\ 0.0000 & 0.0000 & 0.0750 & 0.0000 & 0.0000 & 0.0000 & 0.0000 & 0.0003 \\ 0.0003 & 0.0000 & 0.0000 & 0.0000 & 0.0000 & 0.0250 & 0.1250 & 0.0000 \\ 0.0000 & 0.0003 & 0.0000 & 0.0000 & 0.0750 & 0.0000 & 0.1000 & 0.0000 \\ 0.0000 & 0.0000 & 0.0333 & 0.0000 & 0.0750 & 0.1500 & 0.0000 & 0.0750 \\ 0.0000 & 0.0000 & 0.0000 & 0.0333 & 0.0000 & 0.0000 & 0.0750 & 0.0000 \end{bmatrix} \tag{11}$$

4. OBJECTIVE FUNCTIONS

Four technical and economical objective functions are taken into account for optimum control and generation dispatching purposes. These functions include reliability, *EGC*, *GL* and *VP*. Subsequently, an *FMOF* was developed to optimize simultaneously the functions above.

4.1. Reliability objective function

The function is defined based on a couple of indices, i.e. relative expected energy not supplied (*EENS*) and relative system average interruption frequency index (*SAIFI*). The resultant index is called here energy and average interruption frequency index (*EAIFI*). Since some smart grids have got looped structure, therefore corresponding reliability calculation is carried out by the minimal cut-set method. Subsequently, the minimal cut-sets, which interrupt generated power to each load point, are fully identified. The failure rate, unavailability and repair time attributed to each load point are computed as follows [24]:

$$\lambda_i = \sum \lambda_j \tag{12}$$

$$u_i = \sum_j \lambda_j r_j \tag{13}$$

$$r_i = \frac{u_i}{\lambda_i} \tag{14}$$

where λ_i and r_i indicate failure rate and repair time of load point i, respectively, λ_j and r_j ascertain failure rate and mean outage time of cut-set j, respectively, and u_i indicates unavailability of load point i that can be interpreted as the mean time during a calendar year in which load point i is not energized.

The *SAIFI* is defined as below:

$$SAIFI = \frac{\sum_{i=1}^{N_{LP}} \lambda_i N_i}{N_{TC}} \tag{15}$$

where N_{LP}, N_i and N_{TC} denote to be the quantity of load points, the number of consumers in load point i and total number of consumers in the smart grid, respectively.

To compute the *EENS*, a capacity outage probability table is utilized for each load point [24]. The *EENS* of each load point equates to cumulative expectation of energy curtailed for the same load point. The *EENS* of the smart grid is equal to the sum of *EENS* at all load points.

The suggested *EIAFI* is given by:

$$EAIFI = r_1 \frac{EENS}{EENS_{max}} + r_2 \frac{SAIFI}{SAIFI_{max}} \tag{16}$$

where $EENS_{max}$ represents maximum value of the *EENS*, $SAIFI_{max}$ ascertains maximum value of the *SAIFI* obtained from optimization and r_1 and r_2 are weight coefficients so that $r_1 + r_2 = 1$. Exact values

DOI: 10.1002/etep

of r_1 and r_2 depend on smart grid controller decision and are calculated via either a mathematical or the analytic hierarchy process (*AHP*) methods.

4.2. EGC objective function

The *EGC* objective function consists of operation and maintenance and fuel costs of whole generation units. The *EGC* is usually represented by a quadratic function; hence, the *EGC* is defined according to the following equation:

$$EGC = \sum_{i=1}^{N_{dg}} \left(a_i P_{gi}^2 + b_i P_{gi} + c_i \right) \tag{17}$$

where N_{dg} is the number of *DG* units, a_i, b_i and c_i represent coefficients of *EGC* of *DG* unit i and P_{gi} denotes power generated by *DG* unit i.

4.3. GL objective function

This objective function depends on the power flow and admittance of the lines according to the given expression:

$$GL = \sum_{i=1}^{N_b} \sum_{j=1}^{N_b} P_{ij} \tag{18}$$

where P_{ij} is written as bellow:

$$P_{ij} = U_i^2 Y_{ij} \cos\left(\theta_{ij}\right) - U_i U_j Y_{ij} cos\left(\delta_i - \delta_j - \theta_{ij}\right) \tag{19}$$

where N_b denotes to be the number of lines, U_i and U_j are voltage of end nodes in line i, δ_i and δ_j stand for power angles of end nodes of line i and θ_{ij} is angle of admittance between node i and node j.

4.4. VP objective function

This objective function is defined as Equation (20).

$$VP = \max\left(U_j - U_{ref,j}\right)^2 \tag{20}$$

where U_j and $U_{ref,j}$ are voltage dimension and reference voltage of node j.

This correlation is applied for both radial and looped structures of grids.

5. THE FMOF DESCRIPTION

A fuzzification procedure optimizes the multiple objective functions. This approach transforms elements of the multi-objective function into a fuzzy domain with membership functions. The latter indicate the satisfaction degree of the objectives. A lower membership value implies greater satisfaction with the solution. The shape of membership function depends on the nature of the related objective. Thus, the previously mentioned four objective functions are transformed into fuzzy environment and a single *FMOF* is formulated as follows:

$$\text{Minimize } FMOF = w_1 \psi_1 + w_2 \psi_2 + w_3 \psi_3 + w_4 \psi_4 \tag{21}$$

where ψ_1 to ψ_4 stand for fuzzy subordination of the *EAIFI*, *EGC*, *GL* and *VP*, respectively, and w_1 to w_4 are weight coefficients so that sum of w_1 to w_4 is equal to unity. Exact value of each weight coefficient depends on the smart grid controller decision, which could be calculated by the *AHP* method.

The basic purpose of reliability membership function is to obtain the minimum value of the *EAIFI*. Because the exponential function meets this criterion, the membership function for reliability improvement is expressed as follows:

DOI: 10.1002/etep

$$\psi_1 = \begin{cases} 0 & EAIFI \leq EAIFI_{best} \\ 1 - exp\left(\dfrac{EAIFI_{best} - EAIFI}{EAIFI_{best}}\right) & EAIFI > EAIFI_{best} \end{cases} \tag{22}$$

where $EAIFI_{best}$ is the best value (the least value which is numerically extracted) obtained from optimizing the *EAIFI*.

The *EGC* and *GL* fuzzified functions are expressed by a linear partition function of rise half trapezoid given by:

$$\psi_2 = \begin{cases} 0 & EGC \leq EGC_{best} \\ \dfrac{EGC - EGC_{best}}{EGC_{max} - EGC_{best}} & EGC_{best} < EGC < EGC_{max} \\ 1 & EGC \geq EGC_{max} \end{cases} \tag{23}$$

where EGC_{max} is the upper limit value of the *EGC* objective function and EGC_{best} ascertains the best value of the *EGC* acquired from the *EGC* objective function's optimization.

The *EGC* fuzzified function is given by a linear partition function of rise half trapezoid according to the following equation:

$$\psi_3 = \begin{cases} 0 & GL \leq GL_{best} \\ \dfrac{GL - GL_{best}}{GL_{max} - GL_{best}} & GL_{best} < GL < GL_{max} \\ 1 & GL \geq GL_{max} \end{cases} \tag{24}$$

where, GL_{max} is upper limit value of the *GL* objective function, and GL_{best} is the best value of the *GL* obtained from the *GL* objective function' optimization.

Since *VP* was related to the square of voltage change values, a root function was chosen to modify fuzzified *VP* such that:

$$\psi_4 = \begin{cases} 0 & VP \leq VP_{best} \\ \sqrt{\dfrac{VP - VP_{best}}{VP_{max} - VP_{best}}} & VP_{best} < VP < VP_{max} \\ 1 & VP \geq VP_{max} \end{cases} \tag{25}$$

where VP_{max} and VP_{best} stand for the upper limit value of the *VP* and the best value obtained from optimization of the *VP*, respectively.

6. PROBLEM CONSTRAINTS

The electric network should satisfy several definite security and configuration constraints during the optimization process of generation dispatching. These constraints are described as follows:

$$\begin{aligned} & P_{DGi}^{min} \leq P_{DGi} \leq P_{DGi}^{max} \\ & Q_{DGi}^{min} \leq Q_{DGi} \leq Q_{DGi}^{max} \\ & P_{Gi} - P_{Di} = \sum_{j=1}^{Nb} P_{ij} \\ & Q_{Gi} - Q_{Di} = \sum_{j=1}^{Nb} Q_{ij} \\ & |S_l| \leq S_l^{max} \\ & U_i^{min} \leq U_i \leq U_i^{max} \end{aligned} \tag{26}$$

DOI: 10.1002/etep

where P_{DGi}^{min}, P_{DGi}^{max},Q_{DGi}^{min} and Q_{DGi}^{max} are the minimum active power, maximum active power, minimum reactive power and maximum reactive power that could be generated by *DG* unit *i*, respectively. P_{Gi}, P_{Di} and P_{ij} denote the total active power of installed *DG* units on node *i*, total active power demand in node *i* and transmitted active power from node *i* to node *j*, respectively. Q_{Gi} and Q_{Di} stand for the total reactive power of installed *DG* units on node *i* and the total reactive power demand in node *i*, respectively; S_l and S_l^{max} are the apparent power flow in line *l* and the maximum apparent power that can flow in line *l*, respectively. U_i^{min}, U_i^{max} and U_i represent the minimum permitted voltage, maximum permitted voltage and voltage of node *i*, respectively.

Q_{ij} is the transmitted reactive power from node *i* to node *j*:

$$Q_{ij} = U_i^2 Y_{ij} \sin(\theta_{ij}) - U_i U_j Y_{ij} sin(\delta_i - \delta_j - \theta_{ij}) \tag{27}$$

where $Y_{i,j}$ is the admittance between node *i* and node *j*.

7. OPTIMIZATION METHOD

The proposed *SA–PSO* benefits several advantages of *SA* and *PSO* methods together. In order to describe the *SA–PSO* technique, a brief discussion of the *SA* and the *PSO* is given as below:

7.1. SA optimization method

This optimization process is analogous to the way liquid freezes or metal recrystallizes in the annealing. In the latter process, the metal is initially heated up to the melting point. Then, it is slowly cooled down to thermal equilibrium state at each temperature. *SA* has an asymptotic convergence to the global optimization that allows for uphill moves [25,26]. It starts at high temperature T_0 with an initial feasible solution. The temperature is then decreased following a cooling schedule, $\mu(T_0,k)$. In temperature reduction steps, a fixed number of solutions are checked. The best value of the objective is compared to the new one in each solution. If the new solution gives a better objective value than the current one, it would be accepted. However, if the new objective value does not meet the criteria comparing the current one, then it can be accepted with an acceptance probability given by Equation (28) [27] such that:

$$P_{new}(X) = \exp\left(-\frac{f(X_{old}) - f(X_{new})}{\mu(T_0,k)}\right) \tag{28}$$

where $f(X_{new})$ and $f(X_{old})$ are new solution and current objective value, respectively. *k* is the number of iteration. The $\mu(T_0, k)$ represents new temperature.

T_0 is assumed suitable if it results in an average acceptance probability, p_0, to be ~0.95. The value of T_0 depends on the scale of the objective function. Hence, T_0 is estimated by conducting an initial search, at which 95% rise of the objective function is accepted and the maximum objective increment, $\Delta f_{max}(x)$, is calculated and recorded subsequently. Thus, T_0 is given by Equation (29):

$$T_0 = \frac{-\Delta f_{max}(X_0)}{\ln(p_0)} \tag{29}$$

In order to enhance coverage speed of *FMOF*, a logarithmic temperature reduction schedule is defined such that:

$$\mu(T_0,k) = \frac{T_0}{(1 + \log_{T0} k)} \tag{30}$$

7.2. PSO method

This technique is a population-based optimization method, in which each particle represents a candidate solution. If one particle finds a desirable path to proceed, then the other particles of this swarm will follow that. The particle vector modification formula shows several variations according to [28,29]:

DOI: 10.1002/etep

$$V_{ij}^{k+1} = \omega \times V_{ij}^{k} + c_1 \times rand_1 \times \left(P_{best,i}^{k} - X_{ij}^{k}\right) + c_2 \times rand_2 \times \left(G_{best}^{k} - X_{ij}^{k}\right)$$
$$X_{ij}^{k+1} = X_{ij}^{k} + V_{ij}^{k+1} \tag{31}$$
$$i = 1, 2, \ldots, N_{dg}; j = 1, 2, \ldots, N_{swarm}$$

where k is the current iteration number, i is the index of each particle, V_{ij}^{k+1} is the modified velocity vector of particle i based on the three displacement fundamentals, X_{ij}^{k+1} is the updated position of particle i, $rand_1$ and $rand_2$ are random numbers ranging [0,1], c_1 and c_2 ascertain learning factors, $P_{best,i}$ denotes the best previous experience of the particle i that is recorded, G_{best} stands for the best previous experience of among the entire population, N_{dg} is the number of particles, N_{swarm} ascertains the number of swarms and ω denotes the inertia or momentum weight factor.

7.3. SA–PSO method

However, high convergence speed and robustness can be considered as two important advantages of the *PSO* method, it gives rise to local optima trapping. We propose the *SA–PSO* method to use global optimization advantage of the *SA* technique in order to reduce the local optima trapping. Regarding sections 7.1 and 7.2, the procedure for implementing the proposed *SA–PSO* method for the generation dispatching is categorized in several steps:

Step 1: Initializing temperature and a population of particles with random positions and velocities in the N_{swarm}-dimensional problem space using a uniform probability distribution function at *iteration* = 1;
Step 2: Considering particle i and running *AC* load flow;
Step 3: Checking constraints; if the constraints are not satisfied, then do not accept new position and velocity of the particle and go to step 2;
Step 4: Calculating reliability, *VP*, *GL* and *EGC* indices; if each of the $EAIFI_{best}$, EGC_{best}, GL_{best} or VP_{best} becomes lower than their last value, take their new quantities and set *iteration* = 1; then, go to Step 2;
Step 5: Calculating *FMOF* (fitness) for each particle;
Step 6: Comparing particle's fitness with its own, $P_{best,i}$. If the current value is lower than the $P_{best,i}$, then, set $P_{best,i}$ value equal to the current location in N_{swarm}-dimensional space;
Step 7: Comparing fitness with the population's overall best previous solution (G_{best}). If the current value is better than G_{best}, then, reset G_{best} to the current particle's array index and value;
Step 8: If the current value of fitness function is not better than $P_{best,i}$, calculate P_{new} from Equation (28). If P_T is larger than a random quantity, then, update velocity and position of the particle according to Equation (31); otherwise, do not accept new position and velocity of the particle and go to step 2;
Step 9: If a predefined stopping criterion such as a sufficiently good fitness or a maximum number of iterations is met, then accept G_{best} as a solution; otherwise, set *iteration* = *itteration* + 1, apply cooling process by Equation (30) and go to step 2.

8. CASE STUDY

Methodologies discussed in previous sections were applied to the smart grid in Figure 9 as a case study.

The installed *DG* units in this case study consist of four renewable types and four fossil fuel types. The DG units containing a *WT*, a *PV*, a hybrid *WT–FC*, a hybrid *PV–FC*, 2 gas engines (*GE1* and *GE2*) and two micro turbines (*MT1* and *MT2*). Table I lists the capacity and location of the *DG* units as well as data of load points.

Data of smart grid power lines are presented in Table II. The generation dispatching was accomplished for the micro grid in a 24-h period of day-ahead. Load duration of each load point during 24-h period of day-ahead is shown in Table III.

DOI: 10.1002/etep

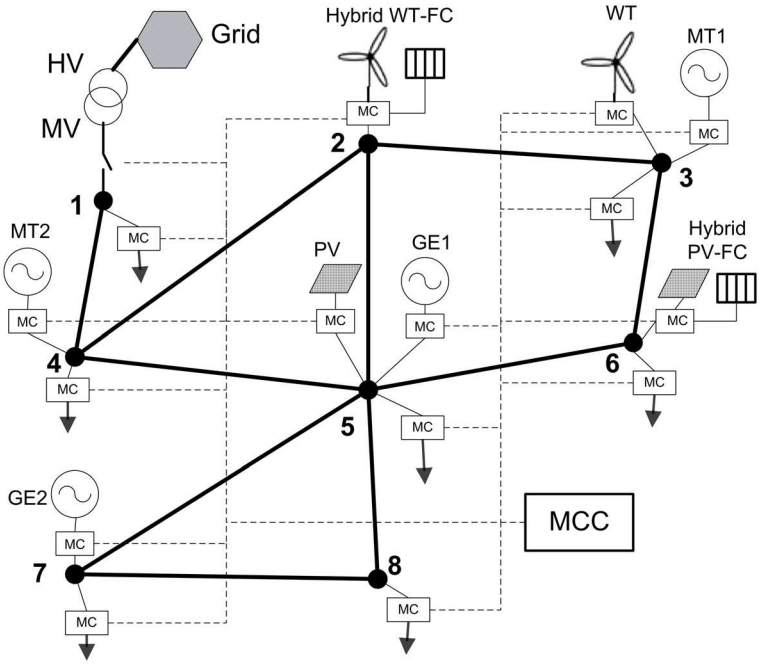

Figure 9. Reliability model of the *PV* unit.

Table I. DG units and data of load points.

	First installed DG unit		Second installed DG unit		Maximum load		
Node	*DG* name	Capacity (kW)	*DG* name	Capacity (kW)	P_{Max} (kW)	Q_{Max} (kVAR)	Number of consumers
1	–	–	–	–	110	11	16
2	Hybrid WG–FC	650	–	–	–	–	–
3	WG	650	MT1	250	123	27	3
4	MT2	250	–	–	164	16	24
5	PV	350	GE1	750	200	20	31
6	Hybrid PV–FC	350	–	–	176	18	25
7	GE2	750	–	–	200	20	29
8	–	–	–	–	100	10	14

Table II. The data of smart grid power lines.

Line no.	Start node	End node	R (pu)$\times 10^{-3}$	X (pu)$\times 10^{-3}$	B (pu)$\times 10^{-3}$	Failure rate (f/y)
1	1	4	5.68	3.15	0.39	1.36
2	2	3	2.81	1.56	0.20	0.67
3	2	4	5.87	3.26	0.41	1.40
4	2	5	6.93	3.85	0.48	1.65
5	3	6	3.99	2.22	0.28	0.95
6	4	5	2.31	1.28	0.16	0.55
7	5	6	1.37	0.76	0.10	0.33
8	5	7	7.05	3.92	0.49	1.68
9	5	8	4.68	2.60	0.33	1.12
10	7	8	2.81	1.56	0.20	0.67

DOI: 10.1002/etep

Table III. Power demand (kW) in a 24-h period of day-ahead.

	No. of load point													
	1		3		4		5		6		7		8	
Hours	kW	kVar	kW	kVar	kW	kVar	kW	kVar	kW	kVar	kW	kVar	kW	kVar
1	31	5	95	23	82	11	117	15	92	12	121	15	27	5
2	27	3	114	22	47	4	64	6	35	3	64	6	27	2
3	13	1	112	21	32	3	30	3	26	2	30	3	13	1
4	13	1	110	20	32	3	30	3	24	2	30	3	13	1
5	22	2	106	18	39	4	42	4	32	3	42	4	22	2
6	38	4	102	15	74	7	67	7	47	4	67	7	38	3
7	67	7	101	15	94	9	73	7	52	5	73	7	67	7
8	83	8	100	14	98	10	69	7	57	6	69	7	83	8
9	85	8	98	11	99	10	53	5	48	5	53	5	85	8
10	87	9	98	10	117	12	98	10	73	7	98	9	87	9
11	89	9	98	10	119	12	108	11	87	9	108	11	89	10
12	90	9	103	13	121	12	124	12	101	10	124	12	90	9
13	90	9	105	17	114	11	135	13	109	11	135	13	90	9
14	85	8	105	17	87	9	140	14	116	12	140	14	85	8
15	85	8	105	17	96	10	140	14	122	12	140	14	85	8
16	95	10	107	18	112	11	146	15	126	13	146	15	90	9
17	96	10	102	15	134	13	114	11	128	13	114	11	91	9
18	98	10	118	21	157	16	112	11	137	14	112	11	93	9
19	105	11	123	27	164	16	167	16	154	15	167	17	98	10
20	110	11	123	27	164	16	189	19	176	18	189	19	100	10
21	110	11	123	27	164	16	200	20	176	18	200	20	100	10
22	110	11	120	24	163	16	200	20	168	17	200	20	100	10
23	100	10	120	24	152	15	187	19	157	15	187	18	97	9
24	93	9	120	24	134	13	175	18	151	15	175	17	27	9

DOI: 10.1002/etep

9. NUMERICAL RESULTS

Approaches of this study were applied to accomplish generation dispatching of the smart grid. Table IV represents suitable values of decision variables chosen after checking performance of a wide range of quantities for the case study. Table V summarizes the results for generation power dispatching of each *DG* unit as well as the values of objective function indices in the related time intervals of the day-ahead.

The results show that the suggested *SA–PSO* method gives better optimum values of the *FMOF* and execution time is less than the conventional *PSO* method in definite time intervals. Figure 10 illustrates *FMOF* variations by both *SA–PSO* and *PSO* methods. It indicates that the suggested *SA–PSO* method is 3 times faster than the *PSO* method, which is an achievement in smart decision making of power dispatching.

Table IV. Suitable values of decision variables.

Decision variable	Value
r_1	0.8
r_2	0.2
w_1	0.33
w_2	0.11
w_3	0.27
w_4	0.29
N_{swarm}	13
T_0	115

Table V. Optimum generation dispatching of each *DG* unit and the values of objective function indices in the related time intervals of the day-ahead.

	Optimum power dispatching of the DG units (kW)											
Hours	WT	PV	WT–FC	PV–FC	GE1	GE2	MT1	MT2	EAIFI	EGC ($)	GL(kW)	VP
1	421	0	302	251	588	424	109	106	0.22	20.99	44	0.005
2	42	0	279	134	439	459	134	157	0.20	12.44	37	0.007
3	0	0	354	271	526	605	104	112	0.20	8.67	95	0.011
4	0	0	423	313	556	470	117	159	0.20	8.18	39	0.009
5	0	18	155	158	367	638	168	135	0.20	7.68	35	0.006
6	0	1	199	330	638	575	112	115	1.00	7.42	34	0.006
7	0	171	458	301	638	590	121	166	0.30	8.72	34	0.006
8	167	168	525	223	536	638	168	158	0.30	12.04	35	0.006
9	156	31	191	255	352	581	132	0	0.98	16.98	37	0.012
10	188	12	630	84	469	489	120	133	0.98	17.82	36	0.007
11	379	122	284	81	590	600	168	131	0.98	17.40	91	0.011
12	177	99	183	180	479	585	129	168	0.98	73.51	34	0.009
13	0	0	154	0	512	593	168	132	0.99	8.10	32	0.005
14	0	22	365	306	0	599	137	102	0.99	42.00	37	0.005
15	92	123	100	64	552	606	159	120	0.98	9.76	84	0.005
16	0	23	96	153	431	553	143	128	0.99	12.63	36	0.005
17	295	0	242	157	0	584	139	148	1.00	13.39	33	0.005
18	438	0	579	330	0	578	145	154	1.00	12.90	32	0.005
19	116	0	416	249	503	610	149	157	0.99	14.90	31	0.005
20	67	0	575	125	531	593	0	137	0.97	18.00	32	0.005
21	96	0	343	233	425	616	145	168	0.98	45.65	37	0.005
22	410	0	285	212	462	606	115	168	0.98	42.48	30	0.005
23	141	0	598	161	369	344	115	122	0.97	14.13	33	0.008
24	0	0	429	0	0	595	168	0	0.98	33.14	31	0.005

DOI: 10.1002/etep

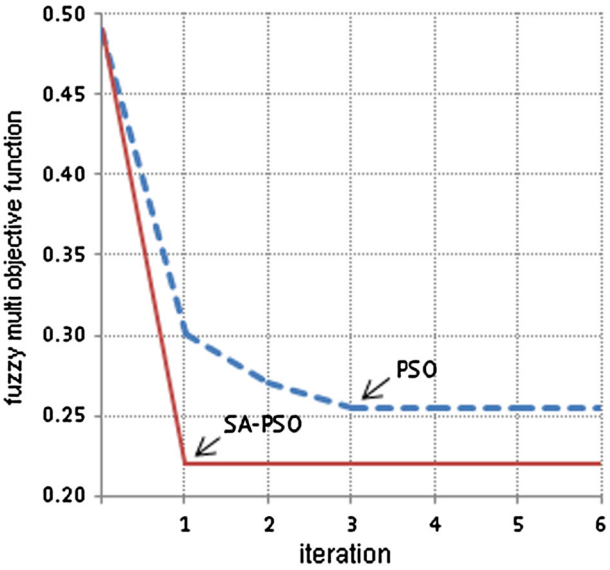

Figure 10. Tracking *FMOF* quantity by *SA–PSO* and *PSO*.

Result changes of the *FMOF* in 24 h of day-ahead are shown in Figure 11.

Relative quantity of electricity generated from each kind of energy resource per maximum capacity of each type of the *DG* units in a 24-h period of the day-ahead is illustrated in Figure 12.

Scenarios including the alteration of wind speed, fuel price, sun light irradiance and weights of objective functions are analyzed accordingly. Initially, the data was acquired from normal scenario. In the next scenarios, change percent of cumulative goal function indices in 24 h of day-ahead was analyzed respect to the normal scenario. These scenario analyses were given as follows:

9.1. Wind speed scenario

Change percent of the cumulative goal function indices in 24 h of day-ahead in both high and low wind speed scenarios in comparison with normal scenario is shown in Figure 13. In high wind speed scenario, the *VPF*, *SAIFI* and *FMOF* were better (lower) than the same indices in the normal scenario. In low wind speed scenario, the *GCF*, *VPF* and *FMOF* exhibit better values than the same indices given by the normal scenario.

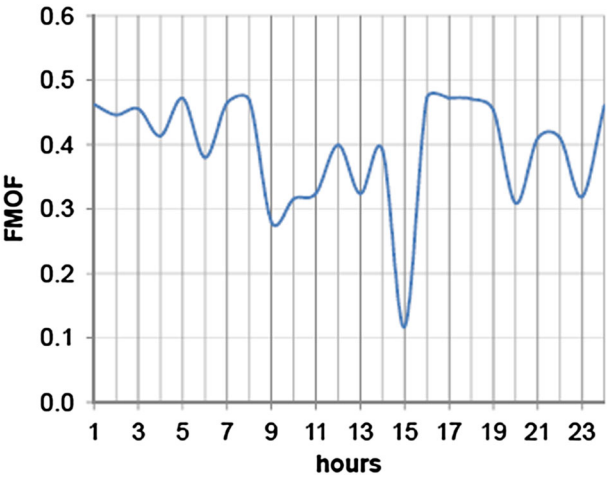

Figure 11. *FMOF* changes on the day-ahead.

DOI: 10.1002/etep

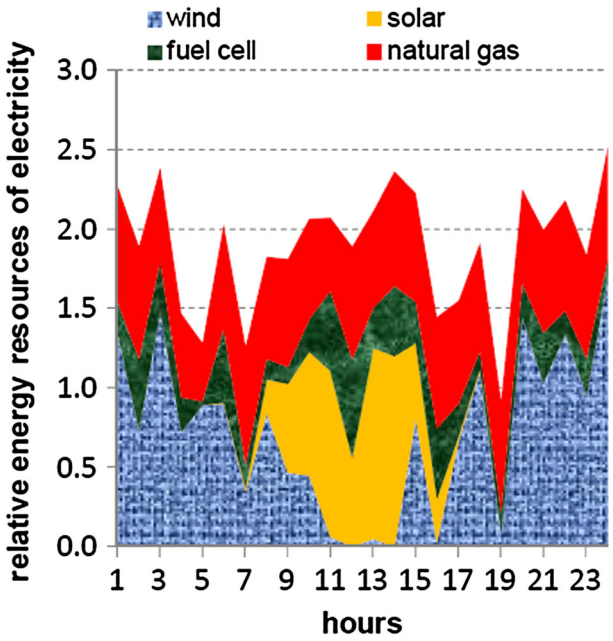

Figure 12. Relative quantity of electricity generation from energy resources.

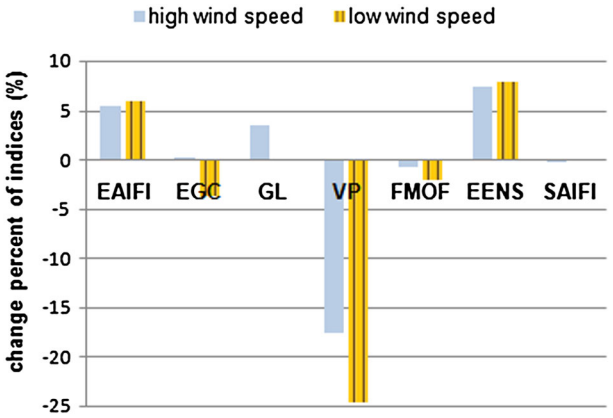

Figure 13. Change percent of cumulative indices in the wind speed scenario in comparison with the normal scenario.

9.2. *Cloudy day scenario*

Figure 14 illustrates change percent of cumulative goal function indices of day-ahead in the cloudy day scenario in comparison with the normal scenario. In the cloudy day scenario, the *EGC*, *GL*, *VP*, *SAIFI* and *FMOF* obtain better values than the same indices given by the normal scenario.

9.3. *Fuel price scenario*

Change percent of cumulative goal function indices in 24 h of day-ahead in high and low fuel price scenarios are demonstrated in Figure 15 in comparison with the normal scenario. In high fuel price scenario, the *EAIFI*, *EGC*, *GL* and *EENS* are found to be worse than the same indices in the normal scenario. In low fuel price scenario, the E*GC*, *VP* and *FMOF* get better than the same indices given in the normal scenario.

9.4. *Reliability weight change scenario*

Figure 16 illustrates the change percent of cumulative goal function indices of day-ahead in high reliability weight scenario and low reliability weight scenario in comparison with the normal scenario.

DOI: 10.1002/etep

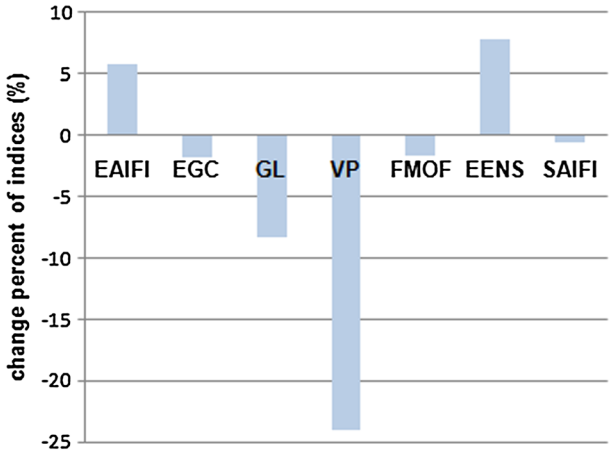

Figure 14. Change percent of cumulative indices in the cloudy day scenario in comparison with the normal scenario.

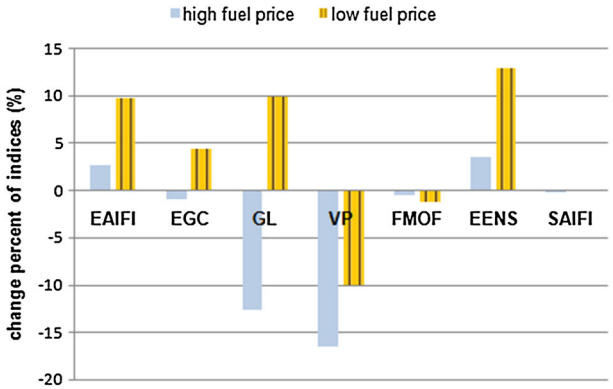

Figure 15. Change percent of cumulative indices in the fuel price scenario in comparison with the normal scenario.

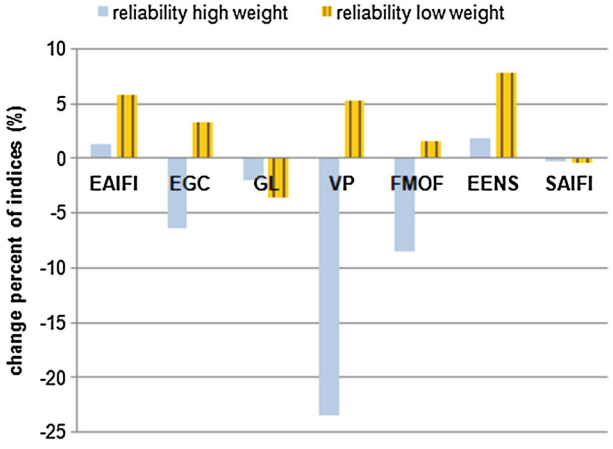

Figure 16. Change percent of goal function indices in reliability weight change scenario in comparison with the normal scenario.

DOI: 10.1002/etep

In the high reliability weight scenario, the *EAIFI* and *EENS* get better than the same indices given in the low reliability weight scenario. The *SAIFI* does not undergo a noticeable change according to the reliability weights.

10. CONCLUSIONS

The proposed reliability models of renewable *DG*s as well as *FMOF* are taken into account as efficient methods to assess uncertainty of the renewable energies providing a smart generation dispatching. The reliability index, *EAIFI*, was developed based on energy and interruption frequency to contribute the optimization generation dispatching in smart grids. The suggested *SA–PSO* method is a faster one to give better results respect to the conventional *PSO* technique within the definite time intervals. Scenario's analyses indicate that 15% rise of average wind speed leads to 5.5% growth of generation cost. In other words, *EGC* not only depends upon energy resources, but also on the grid topology, load points profile, *DG* places and the corresponding capacities. Furthermore, the results demonstrate that 52% increase of the reliability index weight in *FMOF* finds an increment of 1.3% of *EAIFI*; i.e. the greater values of *EAIFI* weight do not necessarily reduce *EAIFI*. Therefore, the changes of each index affect on the other indices and the smart grids structure accordingly. Eventually, this work showed that due to ability of comprehensive control of *DER*s in smart grids they are foreseen to be frequently utilized in the future power systems.

ACKNOWLEDGEMENT

The authors thank Prof. Parviz Parvin, head of Photonic, Energy Engineering and Physics Department of Amirkabir University of Technology, for his useful comments.

11. LIST OF SYMBOLS AND ABBREVIATIONS

A	Sweep area of the wind turbine rotor
a_i	Coefficient of *EGC* of *DG* unit *i*
b_i	Coefficient of *EGC* of *DG* unit *i*
c_i	Coefficient of *EGC* of *DG* unit *i*
c_1	Learning factor 1
c_2	Learning factor 2
c_v	Total efficiency of wind turbine
DG	Distributed generation
EAIFI	Energy and average interruption frequency index
$EAIFI_{best}$	Best value that got from optimizing the *EAIFI*
EENS	Expected energy not supplied
$EENS_{max}$	Maximum value of the *EENS*
EGC	Electricity generation cost function
EGC_{max}	Upper limit value of the *EGC*
f_i	Frequency of occurrence of state *i*
$f(X_{new})$	New solution of objective function
$f(X_{old})$	Current objective value
FMOF	Fuzzy multi-objective function
G_{best}	Best particle among the entire population
GL	Grid loss
N_b	Number of the lines
N_{dg}	Number of *DG* units
N_i	Number of consumers in load point *i*
N_{ij}	Number of observed transitions from state *i* to state *j*
N_{LP}	Number of load points

DOI: 10.1002/etep

N_{states}	Total number of states
N_{swarm}	Number of the particles in the swarm
N_{TC}	Total number of consumers in the smart grid
$P_{best,i}$	Best previous experience of the particle i that is recorded
P_{DGi}^{min}	Minimum active power that could generate by *DG* unit i
P_{DGi}^{max}	Maximum active power that could generate by *DG* unit i
P_{DT}	Total demand of active power
P_{gi}	Generated power by *DG* unit i
P_{GT}	Total active power generated by all *DG* units
P_i	Probability of occurrence of state i
P_{ij}	Transmitted active power from node i to node j
P_{loss}	Grid power losses
P_{new}	Acceptance probability of new objective value
PSO	Particle swarm optimization
p_0	Average acceptance probability
Q_{DGi}	Reactive power generated by *DG* unit i
Q_{DGi}^{min}	Minimum reactive power that could generate by *DG* unit i
Q_{DGi}^{max}	Maximum reactive power that could generate by *DG* unit i
r_1	Weight coefficient
r_2	Weight coefficient
r_i	Repair time of load point i
r_j	Average outage time of cut-set j
$rand_1$	Random number in range of [0,1]
$rand_2$	Random number in range of [0,1]
$Reserve_{min}$	Minimum desired power generation reserve
S_l	Apparent power flow in line l
S_l^{max}	Maximum apparent power that can flow in line l
SA	Simulated annealing
SA–PSO	Simulated annealing hybrid by particle swarm optimization method
SAIFI	System average interruption frequency index
$SAIFI_{max}$	Maximum value of the *SAIFI*
T	Entire period of observation
T_i	Duration of state i calculated during the whole period
T_0	High initial temperature
u_i	Unavailability of load point i
U_i^{min}	Minimum permitted voltage on node i
U_i^{max}	Maximum permitted voltage on node i
U_j	End node voltage of line i
v	Wind speed
v_{in}	Cut-in speed of the wind turbine
V_i	Start node voltage of line i
V_i^{k+1}	Updated velocity vector of particle i
v_{out}	Cut-out speed of the wind turbine
v_r	Rated speed of the wind turbine
$V_{ref,j}$	Reference voltage of node j
VP	Voltage profile
w_1	Weight coefficient
w_2	Weight coefficient
w_3	Weight coefficient
w_4	Weight coefficient
X_i^{k+1}	Updated position of particle i
$Y_{i,j}$	Admittance between node i and node j
$\Delta f_{max}(x)$	Maximum objective increase
δ_i	Power angles of node i

DOI: 10.1002/etep

δ_j	Power angles of node j
λ_{FC}	Transition matrix of the fuel cell
λ_i	Failure rate of load point i
λ_{ij}	Transition rate between states i and j
λ_j	Failure rate of cut-set j
λ_{PV}	Transition matrix of the *PV* unit
λ_{PV-FC}	Transition matrix of the *PV–FC* unit
λ_{WT}	Transition matrix of wind turbine
λ_{WT-FC}	Transition matrix of the *WT–FC* unit
λ_{+i}	Departure rate from state i to the upper state
λ_{-i}	Departure rate from state i to the lower state
μ	Cooling schedule
ω	Inertia or momentum weight factor
ρ	Air density
ψ_1	Fuzzy subordination of the *EAIFI*
ψ_2	Fuzzy subordination of the *EGC*
ψ_3	Fuzzy subordination of the *GL*
ψ_4	Fuzzy subordination of the *VP*
θ_{ij}	Angle of admittance between node i and node j

REFERENCES

1. Aghaei J, Alizadeh I. Demand response in smart electricity grids equipped with renewable energy sources: A review. *Renewable and Sustainable Energy Reviews* 2013; **18**:64–72.
2. Anvari A, Seifi A, Niknam T. Multi-operation management of a typical micro-grids using Particle Swarm Optimization: A comparative study. *Renewable and Sustainable Energy Reviews* 2012; **16**:1268–1281.
3. Ustun TS, Ozansoy C, Zayegh A. Recent developments in microgrids and example cases around the world—A review. *Renewable and Sustainable Energy Reviews* 2011; **15**:4030–4041.
4. Zamora R, Srivastava AK. Controls for microgrids with storage: Review, challenges, and research needs. *Renewable and Sustainable Energy Reviews* 2010; **14**:2009–2018.
5. Lidula NWA, Rajapakse AD. Microgrids research: A review of experimental microgrids and test systems. *Renewable and Sustainable Energy Reviews* 2011; **15**:186–202.
6. Dobakhshari AS, M Fotuhi-firuzabad. A reliability model of large wind farms for power system adequacy studies. *Energy Conversion, IEEE Transactions on* 2009; **24**:792–801.
7. Goleijani S, Ghanbarzadeh T, Sadeghi Nikoo F, Parsa Moghaddam M. Reliability constrained unit commitment in smart grid environment. *Electric Power Systems Research* 2013; **97**:100–108.
8. Marzband M, Sumper A, Domínguez-García JL, Gumara-Ferret R. Experimental validation of a real time energy management system for microgrids in islanded mode using a local day-ahead electricity market and MINLP. *Energy Conversion and Management* 2013; **76**:314–322.
9. Marzband M, Sumper A, Ruiz-Álvarez A, Domínguez-García JL, Tomoiagă B. Experimental evaluation of a real time energy management system for stand-alone microgrids in day-ahead markets. *Applied Energy* 2013; **106**:365–376.
10. Abou El-Ela AA, Fetouh T, Bishr MA, Saleh RAF. Power systems operation using particle swarm optimization technique. *Electric Power Systems Research* 2008; **78**:1906–1913.
11. Baños R, Manzano-Agugliaro F, Montoya FG, Gil C, Alcayde A, Gómez J. Optimization methods applied to renewable and sustainable energy: A review. *Renewable and Sustainable Energy Reviews* 2011; **15**:1753–1766.
12. Marnay C, Venkataramanan G, Stadler M, Siddiqui AS, Firestone R, Chandran B. Optimal technology selection and operation of commercial-building microgrids. *Power Systems, IEEE Transactions on* 2008; **23**:975–982.
13. Chen C, Duan S, Cai T, Liu B, Hu G. Smart energy management system for optimal microgrid economic operation. *IET Renewable Power Generation* 2001; **5**:258.
14. Castro Sayas F, Allan RNN. Generation availability assessment of wind farms. *IEE Proceedings in Generation, Transmission and Distribution* 1996; **143**:507–518.
15. Billinton R, Allan RN. *Reliability evaluation of engineering systems*, 2nd edn. Plenum Press: New York, 1992.
16. Reddy KN, Agarwal V. Utility-Interactive Hybrid Distributed Generation Scheme With Compensation Feature. *Energy Conversion, IEEE Transactions on* 2007; **22**:666–673.
17. Matevosyan J, Soder L. Minimization of imbalance cost trading wind power on the short-term power market. *Power Systems, IEEE Transactions on* 2006; **21**:1396–1404.
18. Durisch W, Bitnar B, Mayor JC, Kiess H, Lam K, Close J. Efficiency model for photovoltaic modules and demonstration of its application to energy yield estimation. *Solar energy materials and solar cells* 2007; **91**:79–84.

DOI: 10.1002/etep

19. Parida B, Iniyan S, Goic R. A review of solar photovoltaic technologies. *Renewable and Sustainable Energy Reviews* 2011; **15**:1625–1636.
20. Deshmukh MK, Deshmukh SS. Modeling of hybrid renewable energy systems. *Renewable and Sustainable Energy Reviews* 2008; **12**:235–249.
21. Poullikkas A. Implementation of distributed generation technologies in isolated power systems. *Renewable and Sustainable Energy Reviews* 2007; **11**:30–56.
22. Lazarov V, Notton G, Stoyanov L. Grid-connected multi-source system sizing. … *Systems & Electric Drives* …, no. July, 2009; pp. 1–5.
23. Ghasemi N, Abedi M, Rastegar H, Gharepetian G. Hybrid distributed generation units PEM fuel cell and microturbine. *Industrial Technology, ICIT IEEE International Conference on* 2008.
24. Billinton R, Allan RN. *Reliability evaluation of power systems*, 2nd edn. Plenum Press: New York, 1996.
25. Niknam T, Meymand HZ, Mojarrad HD. An efficient algorithm for multi-objective optimal operation management of distribution network considering fuel cell power plants. *Energy* 2011; **36**:119–132.
26. Sadegheih A. Optimization of network planning by the novel hybrid algorithms of intelligent optimization techniques. *Energy* 2009; **34**:1539–1551.
27. Vallem MR, Mitra J. Siting and sizing of distributed generation for optimal microgrid architecture. *Power Symposium, Proceedings of the 37th Annual North American* 2005.
28. Kennedy J, Eberhart R. Particle swarm optimization. *Neural Networks, Proceedings, IEEE International Conference on* 1995; **4**:1942–1948.
29. Trelea IC. The particle swarm optimization algorithm: convergence analysis and parameter selection. *Information processing letters* 2003; **85**:317–325.

DOI: 10.1002/etep

International Transactions on Electrical Energy Systems

Edited By: Deqiang Gan, Olav B. Fosso, Badrul H. Chowdhury

Impact Factor: 0.63

ISI Journal Citation Reports © Ranking: 2012: 175/243 (Engineering Electrical & Electronic)

Online ISSN: 2050-7038

Recently Published Issues

See all (/journal/10.1002/(ISSN)2050-7038/issues)

- Current Issue:May 2014 (/doi/10.1002/etep.v24.5/issuetoc)

  Volume 24, Issue 5
- April 2014 (/doi/10.1002/etep.v24.4/issuetoc)

  Volume 24, Issue 4
- March 2014 (/doi/10.1002/etep.v24.3/issuetoc)

  Volume 24, Issue 3
- February 2014 (/doi/10.1002/etep.v24.2/issuetoc)

  Volume 24, Issue 2
- January 2014 (/doi/10.1002/etep.v24.1/issuetoc)

  Volume 24, Issue 1

Connect with Wiley Energy on social media!

Like **Wiley Energy on Facebook (https://www.facebook.com/WileyEnergy)** and follow **Wiley Energy on Twitter (https://twitter.com/wileyenergy)** for solar energy, photovoltaics, wind energy, climate change and bioenergy news, as well as special offers, key research announcements, and industry updates. Click on the links below visit our pages and learn more.

 (https://www.facebook.com/WileyEnergy)
 (https://twitter.com/wileyenergy)

(https://www.facebook.com/pages/Wiley-Energy/262095090501840)

(https://twitter.com/wileyenergy)

European Transactions on Electrical Power

International Transactions on Electrical Energy Systems publishes original research results on key advances in the generation, transmission, and distribution of electrical energy systems. Of particular interest are submissions concerning the modeling, analysis, optimization and control of advanced electric power systems.

New Editor as of January 2014

Welcome to **Badrul H. Chowdhury** (UNC Charlotte), who joins Deqiang Gan and Olav Fosso as Editor of *International Transactions on Electrical Energy Systems*.

Professor Chowdhury replaces Mariesa Crow, who has taken the position of Vice-President of Publications for the IEEE PES, but remains a valued member of our Editorial board.

For the full editorial board details, click here (http://onlinelibrary.wiley.com/journal/10.1002/(ISSN)1546-3109/homepage/EditorialBoard.html).

European Transactions on Electrical Power

Publisher: Verband Deutscher Elektrotechniker; Convention of National Societies of Electrical Engineers of Western Europe; Commission of the European Communities; Convention of National Societies of Electrical Engineers of Europe, John Wiley & Sons

DESCRIPTION

Impact factor	0.63
5-year impact	0.58
Cited half-life	3.60
Immediacy index	0.23
Eigenfactor	0.00
Article influence	0.19
Other titles	European transactions on electrical power (Online), European transactions on electrical power, Electrical power, ETEP
ISSN	1546-3109
OCLC	52964457